Available online at www.sciencedirect.com
ScienceDirect
Ceramics International 37 (2011) 2081–2087
CERAMICS INTERNATIONAL
www.elsevier.com/locate/ceramint

Study of color change and microstructure development of Al_2O_3–Cr_2O_3/Cr_3C_2 nanocomposites prepared by spark plasma sintering

Hao-Tung Lin [a], Bo-Zon Liu [b], Wei-hsio Chen [b], Jow-Lay Huang [b,*], Pramoda K. Nayak [b]

[a] *Electrical Technology Center, Cheng Shiu University, Kaohsiung County 833, Taiwan, ROC*
[b] *Department of Materials Science and Engineering, National Cheng-Kung University, Tainan 701, Taiwan, ROC*

Received 25 November 2010; received in revised form 16 December 2010; accepted 14 February 2011
Available online 29 March 2011

Abstract

The densification behaviors of Al_2O_3–Cr_2O_3/Cr_3C_2 nanocomposites prepared by a Spark Plasma Sintering (SPS) were investigated in this work. The initial powders used for sintering were Al_2O_3–Cr_2O_3, which were prepared by metal organic chemical vapor deposition (MOCVD) in a spout bed. Different colors of the compacts such as green, purple and black were observed after densification process at different SPS temperatures from 1200 °C to 1350 °C. These changes of color were relevant to the existence of secondary phase of green Cr_2O_3, pink solid solution of Cr_2O_3–Al_2O_3 and black Cr_3C_2, which were formed under the different SPS temperature. The secondary phase of Cr_2O_3 retarded the processing of densification for spark plasma sintering at 1200 °C. The Cr_2O_3 reacted with Al_2O_3 to form solid solution of Cr_2O_3–Al_2O_3 and with carbon to form Cr_3C_2 as sintering temperature increased to 1350 °C. The characteristics of high heating rate, shorter sintering time for SPS and the formation of secondary phase of Cr_3C_2 effectively reduced the substrate's grain growth, making Al_2O_3–Cr_2O_3/Cr_3C_2 nanocomposites with small grain size.

Keywords: Alumina; Spark plasma sintering; Chemical vapor deposition

1. Introduction

Compared with conventional hot pressed sintering, spark plasma sintering (SPS) has recently attracted increasing interest due to its ability of rapidly heating the powder compact to high temperatures and consolidating it to high densities within very short time. SPS utilizes applied pressure along with temperature and a pulsed direct current to densify materials. SPS is heralded for its promise in retaining nanostructure features, producing grain boundaries devoid of impurities as well as many other benefits [1–3].

Alumina (Al_2O_3) is one of the most widely used ceramic materials because of its excellent physical, thermal and chemical properties. But the inherently low fracture toughness limits its application. The incorporation of hard particulate reinforcement has widely been used to toughening it. The carbides are good reinforcement materials for oxide ceramics due to their high melting point, high hardness, high Young modulus and wear resistance. Among the carbides, the utilization of Cr_3C_2 as the secondary phase, has led to significant improvement in mechanical properties concomitant with enhanced resistance to high temperature oxidation of Cr_3C_2/Al_2O_3 composites [4–9].

Besides second phase particles, solid solution strengthening is another mechanism for the Al_2O_3 matrix. Chromia (Cr_2O_3) has been used to improve the physical properties of Al_2O_3 [10–14]. As Cr_2O_3 has the same corundum crystal structure as Al_2O_3, Al_2O_3–Cr_2O_3 can form substitution solid solution in all ranges at high temperature. The addition of Cr_2O_3 was found to increase the hardness, tensile strength, and thermal shock resistance of Al_2O_3.

A manufacturing method to provide solid–solution and second reinforced carbide particles was introduced in this study. The nanocomposites of nanosized Cr_2O_3 coated on Al_2O_3 have been prepared by taking $Cr(CO)_6$ as a precursor and Al_2O_3 powders as matrix using metal organic chemical vapor deposition (MOCVD) in a spouted chamber [15]. According to our previous study [16], besides Cr_2O_3, the compositions of decomposed $Cr(CO)_6$ included free carbon. Cr_2O_3 reacted with Al_2O_3 to form Al_2O_3–Cr_2O_3 solid solution and reacted with

* Corresponding author.
E-mail address: jlh888@mail.ncku.edu.tw (J.-L. Huang).

0272-8842/$36.00
doi:10.1016/j.ceramint.2011.02.018

carbon to form carbide. Both of these two reactions took place in the hot pressed (HP) densification process. Due to a longer sintering cycle time, a larger Al_2O_3 grain was observed in the compact with mainly solid solution of Al_2O_3–Cr_2O_3 after the sintering treatment. In order to reduce the Al_2O_3 grain size, the conventional HP densification process was replaced by using a spark plasma sintering (SPS) in this study.

In this report, the interesting phenomenon was observed that the color of the appearance of the compacts changed with the SPS temperature. Furthermore, the sintering shrinkage behavior and the microstructure of the Al_2O_3–Cr_2O_3/Cr–carbide nanocomposites prepared under different SPS conditions were discussed here.

2. Experimental details

2.1. Preparation of composite powders

α-Alumina (α-Al_2O_3, 99.99%, Taimei Chemicals Co. Ltd., Japan) with average grain size 150 nm was used as the matrix in this study. Chromium hexacarbonyl ($Cr(CO)_6$, 99%, Strem Chemicals Co., USA) was used as the precursor of chromium oxide in a MOCVD process. $Cr(CO)_6$ was initially heated for evaporation at 75 °C. Inert He gas was used as the carrier gas for transporting these precursor vapors, into the reaction chamber in a spouted bed. The nanosized composite powders fabricated in the spouted bed for 30 and 60 min were named as S-30 and S-60, respectively. The pressure of reaction chamber was kept at 1333 Pa, and the reaction temperature was kept at 300 °C.

2.2. Densification

The spouted powders were densified by a SPS process (SPS-515S, Sumitomo, Japan). The 1.5 g of powder (pure Al_2O_3, S-30, S-60) were put into a graphite mold of 15.5 mm diameter. The uniaxial pressure of 50 MPa was imposed on the powder and the vacuum level was less than 6 Pa. The heating rate from room temperature to 600 °C and from 600 °C to sintering temperature was 200 °C/min, 100 °C/min, respectively with a holding time of 10 min. There were four different sintering temperature conditions of 1200 °C, 1250 °C, 1300 °C and 1350 °C conducted in this study.

2.3. Characterization

X-ray diffractometry (Regaku D/max-II B, Japan) was used to identify the phases of as-received and carbothermal powders. The microstructures and composition were characterized by field emission gun scanning transmission electron microscopy (FEG-STEM, FEI Tecnai G2 F20, Netherlands) and field emission scanning electron microscope (FESEM, PHILIPS XL40, Netherlands) equipped with energy dispersive X-ray detector (EDS).

3. Results and discussion

3.1. Effect of SPS sintering temperature on the color changes of compacts

The amorphous and nanosized Cr_2O_3 particles coated on Al_2O_3 matrix powder were observed as shown in Fig. 1. The presence of Cu is the contribution from the Cu grid. According to the detailed analysis reported in our previous paper [16], the main composition of the decomposed precursor $Cr(CO)_6$ prepared by MOCVD in a spouted bed were Cr_2O_3 and carbon.

The color of the as spouted powder and compacts prepared under different SPS conditions was shown in Fig. 2. It is observed that the color of compacts sintered at 1200 °C was green; the color of 1250 °C compact was purple; while that of 1300 °C and 1350 °C became black. Fig. 3 indicates the XRD patterns of the as spouted powder and compacts processed by various SPS conditions. Besides Al_2O_3 peaks, the Cr_2O_3 peaks were found in the compact sintered at 1200 °C. Compared with the peak of pure-Al_2O_3, the Al_2O_3 peaks of compact sintered at higher temperature had slight shift to lower angles. It meant only a little solid–solution of Al_2O_3–Cr_2O_3 formed in this compact. This result was special to the compacts fabricated by conventional densification methods in which significant pink

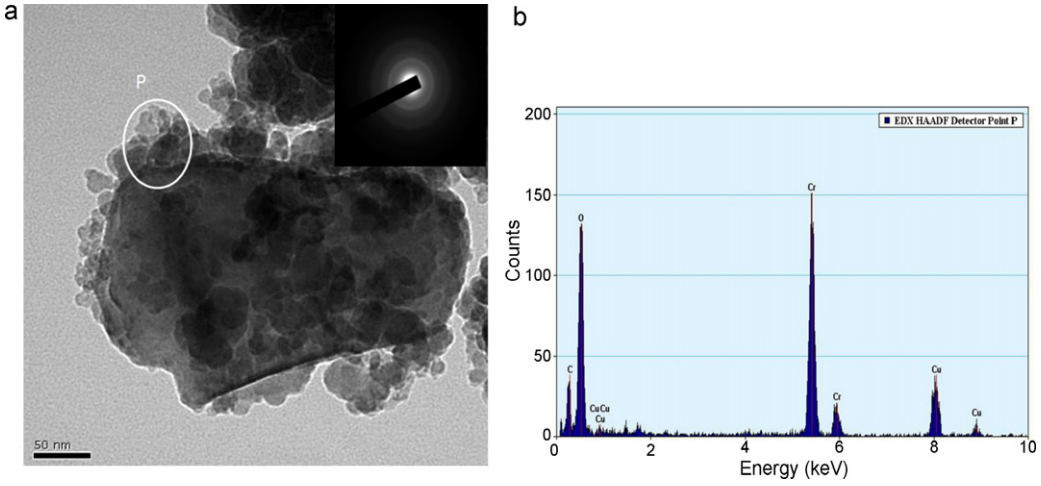

Fig. 1. (a) TEM image of the composite powder prepared in a spouted bed and (b) EDS of the nanosized powder P in (a).

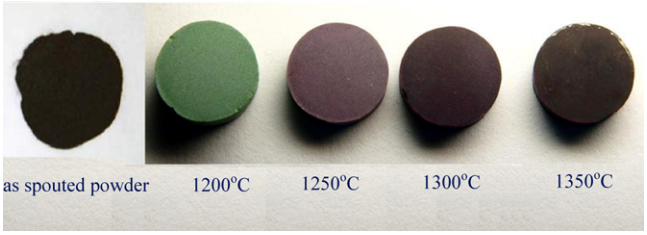

Fig. 2. Optical micrograph of as spouted powder and compacts prepared by different SPS conditions at temperature from 1200 °C to 1350 °C.

solid–solution of Al_2O_3–Cr_2O_3 was formed. According to Bondioli et al., the complete ranges of Al_2O_3–Cr_2O_3 solid solution were obtained, when the reaction temperature is higher than 1000 °C [17].

It was suggested that due to its higher heating rate and short holding time, the most of Cr^{3+} did not have enough time to diffuse into Al_2O_3 matrix and remained as Cr_2O_3 phase after the SPS processing. The color of pure Cr_2O_3 was green, and so the composite was with green appearance. For the compact sintered at 1250 °C, the Cr_2O_3 peaks were disappeared in the XRD pattern because more Cr_2O_3 reacted with Al_2O_3 matrix to form more pink solid solution in this higher sintering temperature. According to Eq. (1) given in [18], it indicates that chromium carbide will be formed probably when the temperature is higher than 1113 °C. It was believed that there was little black carbide formed when sintered at 1250 °C, so the compact had a purple color. It was reasonable that the more Cr^{3+} diffuse into Al_2O_3 matrix with the increase in sintering temperature. In comparison to other compacts, more Al_2O_3 peaks of the compact sintered 1350 °C shifted to lower angles observed from XRD patterns. It indicated that more solid solution was formed at a higher temperature.

$$3Cr_2O_{3(s)} + 13C_{(s)} \rightarrow 2Cr_3C_{2(s)} + 9CO_{(g)} \quad (1)$$

$$\Delta G^\circ = 261,313.95 - 188.5\,T\,(\text{cal})$$

The black color of the compact prepared at 1350 °C was relevant to the formation of chromium carbide. Cr_3C_2 nanoparticles were observed for the compacts prepared at 1300 °C and 1350 °C. The TEM diffraction pattern shows the particle with Cr_3C_2 phase as shown in Fig. 4. Although the peak of Cr_3C_2 peaks were not obvious in the XRD patterns in Fig. 3, but based on the Eq. (1), sintering at a higher temperature was beneficial to form Cr_3C_2. In our previous study [16], Cr_3C_2

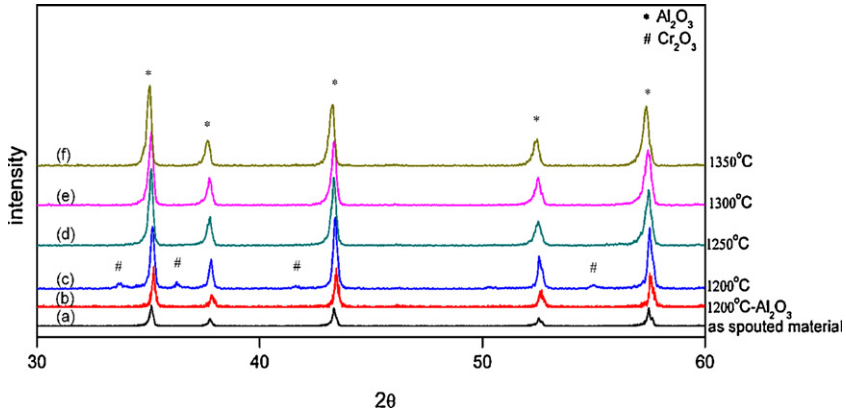

Fig. 3. XRD patterns of (a) as spouted powder (b) pure Al_2O_3 sintered at 1200 °C, and the compacts at (c) 1200 °C, (d) 1250 °C, (e) 1300 °C and (f) 1350 °C for 10 min by SPS.

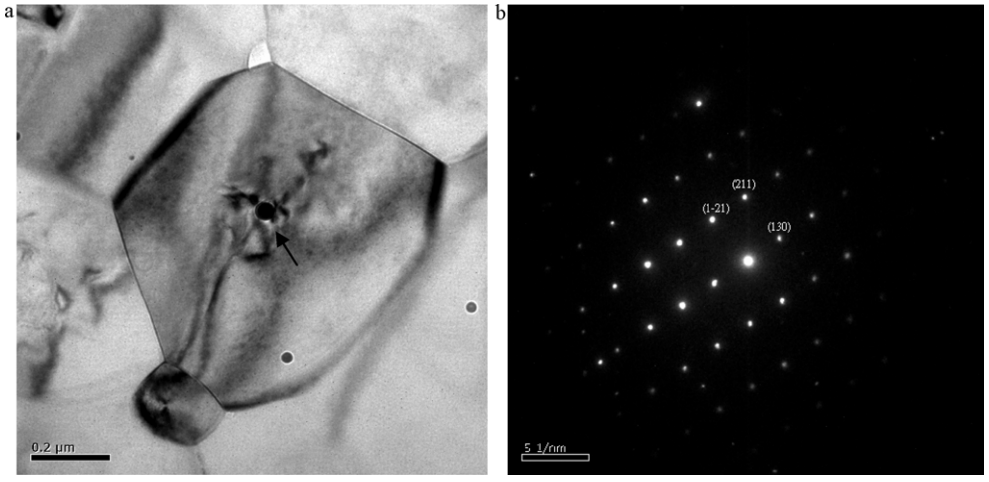

Fig. 4. TEM micrographs of nanocomposites sintered at 1350 °C (a) bright field image and (b) SADP of particle in (a).

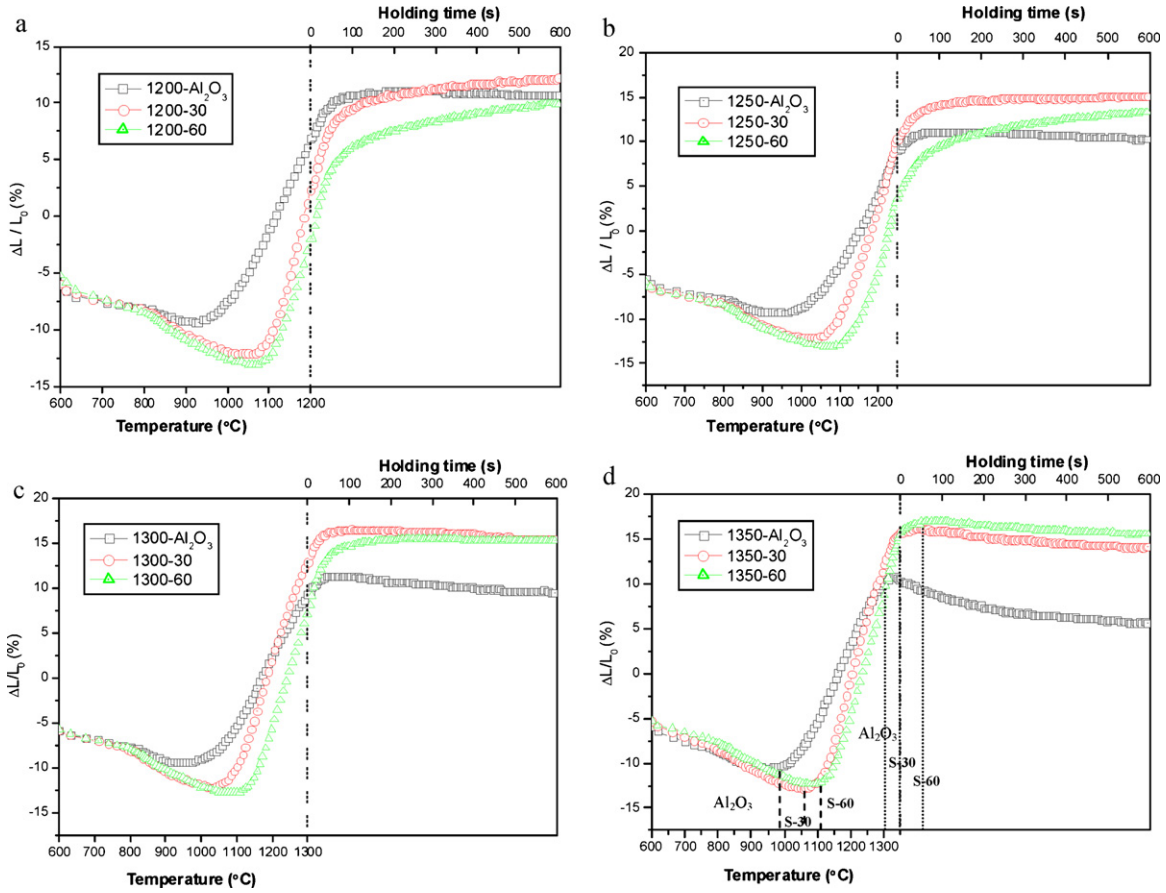

Fig. 5. Sintering shrinkage curves of Al_2O_3, S-30 and S-60 sintered at (a) 1200 °C, (b) 1250 °C, (c) 1300 °C, and (d) 1350 °C for 10 min by SPS.

peaks were easy to be found in the XRD patterns as compacts prepared by HP densification in which the vacuum maintained at about 10^{-3} Pa, however in this SPS process that was about 6 Pa. According to the report of Chu and Ramel [19], due to carbon would be consumed by oxygen in a higher oxygen pressure in SPS process would inhibit the formation of Cr_3C_2.

3.2. Effect of SPS sintering temperature on shrinkage behavior

Fig. 5 shows the sintering shrinkage curves of the pure Al_2O_3, nanocomposite powders of S-30 and S-60 during the SPS densification in the temperature range 1200–1350 °C with holding time of 10 min. The *y*-axis $\Delta L/L_o$ (%) represents the shrinkage profile directly during densification of the powders in real-time. The trend of Al_2O_3 curve became flat at 1200 °C, but the curves of S-30 and S-60 still trended up. This meant the shrinkage Al_2O_3 had already stopped, but S-30 and S-60 continued shrinking during the period of holding time. This result was consistent with the apparent density shown in Fig. 6. It shows the pure Al_2O_3 had a higher density than S-30 and S-60, when the sintering temperature was at 1200 °C and 1250 °C. The amount of shrinkage of S-30 was more significant than S-60. The temperature at which the shrinkage vanished for S-30 and S-60 was 1300 °C and 1350 °C, respectively as shown in Fig. 5(c) and (d). The curves of pure Al_2O_3, S-30 and S-60 were trended down for the holding temperature at 1350 °C. This signifies that all the powder compacts undergone thermal expansion after completion of the sintering shrinkage. The densities of S-30 and S-60 were increased significantly when the temperature raised to 1300 °C and 1350 °C.

Fig. 5(d) illustrates the pure Al_2O_3 started to densify at about 950 °C and finished at about 1300 °C. For S-60 and S-30, the densification temperature started at about 1050 °C and 1100 °C, respectively, and finished at 1350 °C for both. Actually S-60 finished its densification after holding about 50 s. The second

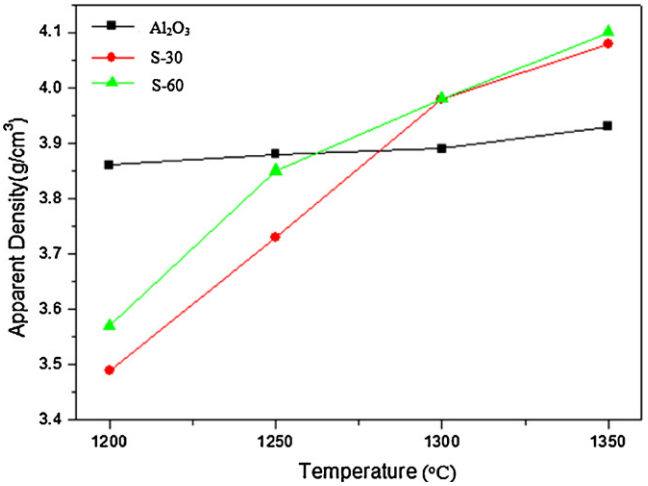

Fig. 6. The apparent density of the specimen of Al_2O_3, S-30, and S-60 prepared at a different SPS sintering temperature from 1200 °C to 1350 °C.

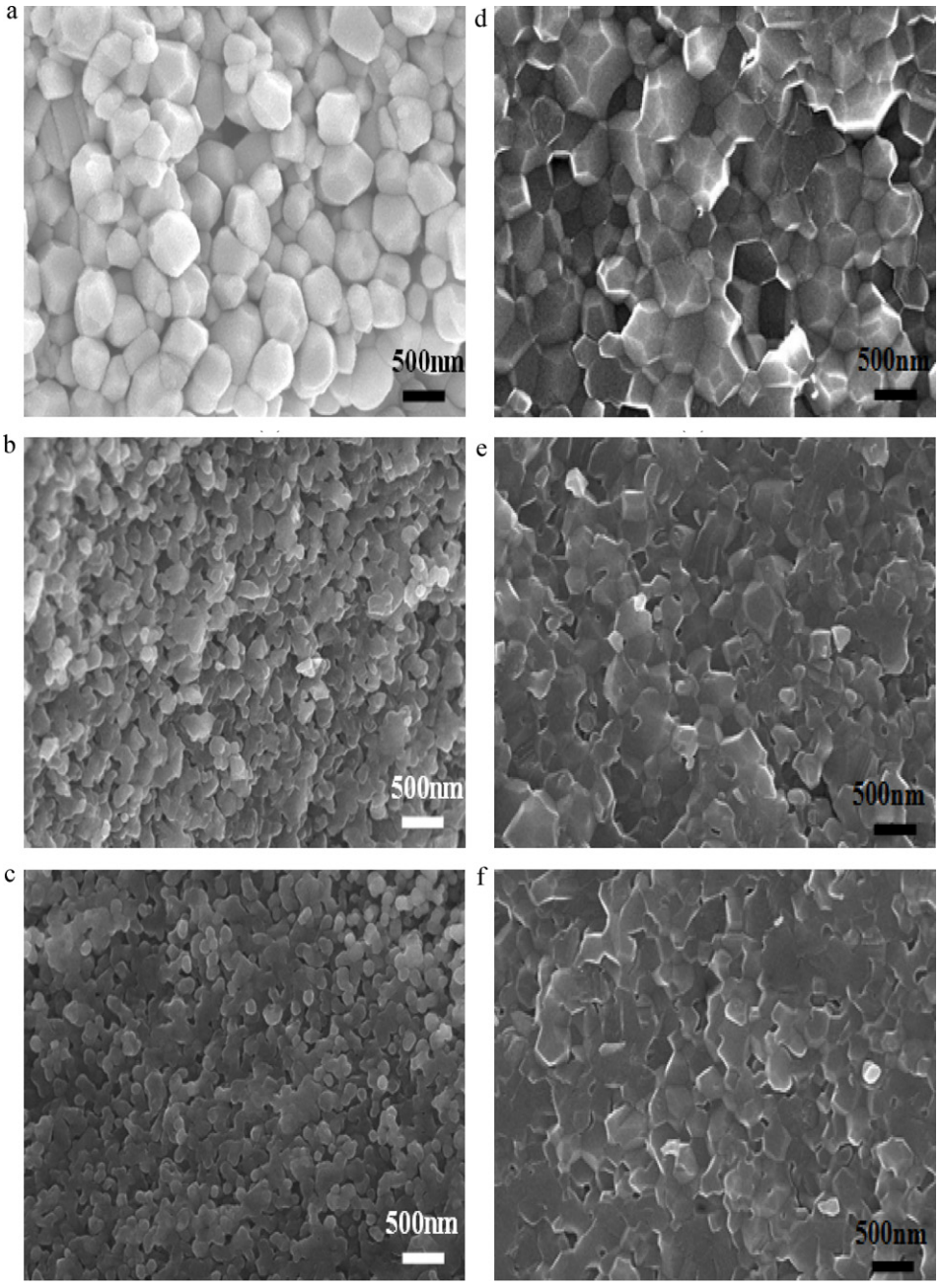

Fig. 7. SEM micrographs of fracture surface of 1200 °C SPS specimen of (a) Al_2O_3, (b) S-30, (c) S-60, and 1250 °C SPS specimen of (d) Al_2O_3, (e) S-30, and (f) S-60.

phase particles decreased the diffusivity of grain boundary and lattice, and resulted in the retardation of densification [20]. According to XRD spectrum shown in Fig. 3, the delay on the densification process for the nanocomposites was due to the Cr_2O_3 particles coating on Al_2O_3 as sintering at 1200 °C. Cr_2O_3 played as a second phase to inhibit the grain growth during densification. When the process temperature was 1300 °C and 1350 °C, the Cr_3C_2 was formed due to higher driving force exerted at higher temperature.

3.3. Effect of SPS sintering temperature on microstructures

The SEM image shown in Fig. 7(a) indicates that the compact of pure Al_2O_3 had a significant grain growth from the raw powder size of 150 nm to about 500 nm when sintered at 1200 °C. However for composites specimen of S-30 and S-60, only the necking between particles were found as shown in Fig. 7(b) and (c).

For the SPS at 1250 °C, most of Cr_2O_3 diffused into Al_2O_3 matrix and formed Al_2O_3–Cr_2O_3 solid solution. A comparison with Fig. 7(a)–(c), the grain growth of the pure Al_2O_3 specimen prepared at 1250 °C was not clear, as shown in Fig. 7(d). However, obvious grain growth was observed on S-30 and S-60 nanocomposites as shown in Fig. 7(e) and (f). It is relevant to the formation of solid solution of Al_2O_3–Cr_2O_3. As chromium ions replaced alumna ions in pure alumina, the resulting expansion of lattice of solid solution tended to lower the bulk modulus [21]. It was suggested that the atoms

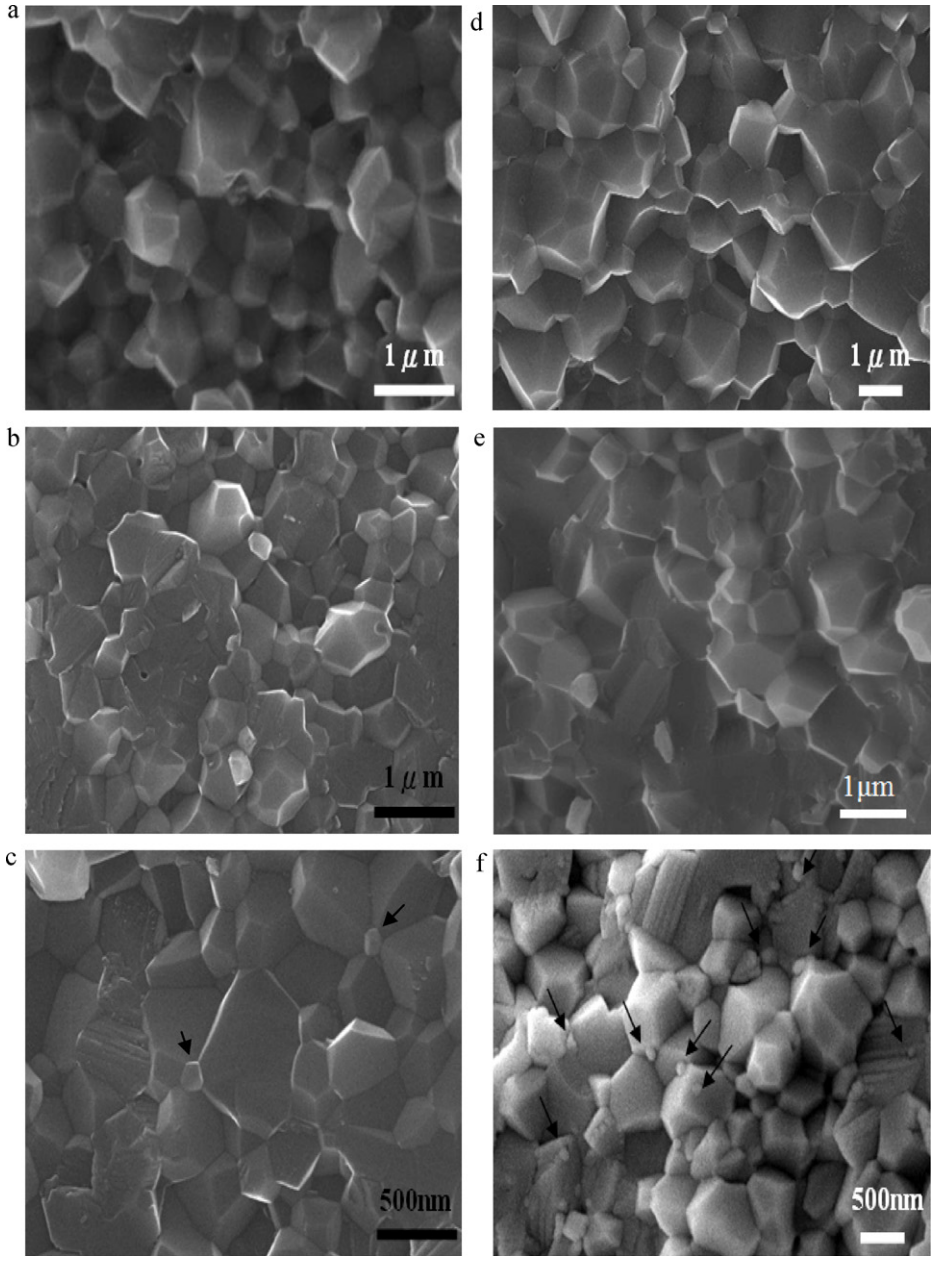

Fig. 8. SEM micrographs of fracture surface of 1300 °C SPS specimen of (a) Al_2O_3, (b) S-30, (c) S-60, and 1350 °C SPS specimen of (d) Al_2O_3, (e) S-30, and (f) S-60.

around the chromium ions have a high diffusion rate [12,15,22].

Fig. 8(a)–(f) shows the SEM images of compacts prepared at 1300 °C and 1350 °C. When sintering temperature was 1350 °C, the grain size of the pure Al_2O_3 was over 1 μm, however that nanocomposites of S-30 and S-60 was about 800–900 nm, as shown in Fig. 8(d)–(f). When sintered at 1300 °C and 1350 °C, the density of composites increased significantly and some nanosized secondary Cr_3C_2 particles with size of about 100 nm were found as shown in Fig. 8(c) and (f). The mean grain size of pure Al_2O_3 compacts became larger and grain growth increased rapidly with increasing sintering temperature. However, for the nanocomposites, the grain growth of Al_2O_3 matrix decreased with the inhibition by second phase particles.

4. Conclusions

The different sintering temperature in SPS process affected the color and microstructures of the Al_2O_3–Cr_2O_3/Cr_3C_2 nanocomposites. The color of specimen changed to green, purple and black as temperature increased from 1200 °C to 1350 °C due to the existence of secondary phase of green Cr_2O_3, pink solid solution of Al_2O_3–Cr_2O_3 and Cr_3C_2 at different temperature. With the increase of sintering temperature, the nanosized coating particles of Cr_2O_3 reacted with Al_2O_3 to form solid solution Al_2O_3–Cr_2O_3 and reacted with carbon to form Cr_3C_2. The shrinkage curves of composites had significantly retarded by the secondary phase particles when compared with pure alumina. The secondary phase particles were Cr_2O_3 when SPS at 1200 °C and it changed to Cr_3C_2 as

temperature increased to 1350 °C. Due to the inhibition from the secondary particles, the nanocomposites had smaller grain size than pure alumina.

Acknowledgement

This study was supported by National Science Council of the Republic of China (R.O.C) under grant no. NSC 99-2923-E-006-002-MY3. The authors would like to thank Institute of Physics, Academia Sinica, Taipei, Taiwan, R.O.C. to carry out SPS measurements.

References

[1] Z. Shen, M. Johnsson, Z. Zhao, M. Nygren, Spark plasma sintering of alumina, J. Am. Ceram. Soc. 85 (8) (2002) 1921–1927.
[2] Z.A. Munir, U. Anselmi-Tamburini, M. Ohyanagi, The effect of electric field and pressure on the synthesis and consolidation of materials: a review of the spark plasma sintering method, J. Mater. Sci. 41 (2006) 763–777.
[3] B.N. Kim, K. Hirga, K. Morita, H. Yoshida, Spark plasma sintering of transparent alumina, Scripta Mater. 57 (2007) 607–610.
[4] J.L. Huang, H.D. Lin, C.A. Jeng, D.F. Lii, Crack growth resistance of Cr_3C_2/Al_2O_3 composites, Mater. Sci. Eng. A 279 (2000) 81–86.
[5] J.L. Huang, K.C. Twu, D.F. Lii, A.K. Li, Investigation of Al_2O_3/Cr_3C_2 composites prepared by pressureless sintering (part 2), Mater. Chem. Phys. 51 (1997) 211–215.
[6] D.F. Lii, J.L. Huang, J.H. Huang, H.H.J. Lu, The interfacial reaction in Cr_3C_2/Al_2O_3 composites, J. Mater. Res. 14 (1999) 817–823.
[7] C.T. Fu, J.M. Wu, A.K. Li, Microstructure and mechanical properties of Cr_3C_2 particulate reinforced Al_2O_3 matrix composites, J. Mater. Sci. 29 (1994) 2671–2677.
[8] C.T. Fu, A.K. Li, J.M. Wu, The effects of oxidation of Cr_3C_2 particle reinforced Al_2O_3 composites on microstructure and mechanical properties, J. Mater. Sci. 28 (1993) 6285–6294.
[9] E.K. Storms, The Refractory Carbides, Academic Press, Inc, New York & London, 1967.
[10] R.C. Bradt, Cr_2O_3 solid solution hardening of Al_2O_3, J. Am. Ceram. Soc. 50 (1967) 54–55.
[11] B.B. Chate, W.C. Smith, C.H. Kim, D.P.H. Hasselman, G.E. Kane, Effect of chromia alloying on machining performance of alumina ceramic cutting tools, Am. Ceram. Soc. Bull. 54 (1975) 210–215.
[12] T.J. Davies, H.G. Emblem, A. Harabi, C.S. Nwobodo, A.A. Ogwu, V. Tsantzlaou, Characterisation and properties of alumina–chrome refractories, Br. Ceram. Trans. 91 (1992) 71–76.
[13] A. Harabi, T.J. Davies, Mechanical properties of sintered alumina chromia refractories, Br. Ceram. Trans. 94 (1995) 79–84.
[14] D.H. Riu, Y.M. Kong, H.E. Kim, Effect of Cr_2O_3 Addition on microstructural evolution and mechanical properties of Al_2O_3, J. Eur. Ceram. Soc. 20 (2000) 1475–1481.
[15] B. Caussat, F.L. Juarez, C. Vahlas, Hydrodynamic study of fine metallic powders in an original spouted bed contactor in view of chemical vapor deposition treatments, Powder Technol. 165 (2006) 65–72.
[16] H.T. Lin, S.C. Wang, J.L. Huang, S.Y. Chang, Processing of hot pressed Al_2O_3–Cr_2O_3/Cr–carbide nanocomposite prepared by MOCVD in a fluidized bed, J. Eur. Ceram. Soc. 27 (2007) 4759–4765.
[17] F. Bondioli, A. Ferrai, C. Leonelli, T. Manfredini, Reaction mechanism in Al_2O_3/chromia (Al_2O_3–Cr_2O_3) solid solution obtained by coprecipitation, J. Am. Ceram. Soc. 83 (2000) 2036–2040.
[18] O. Kubaschewski, E.LL. Evans, C.B. Alcock, Metallurgical Thermochemistry, Pergamon, London, 1979.
[19] W.F. Chu, A. Ramel, The conversion of chromium oxide to chromium carbide, Oxid. Met. 15 (3/4) (1981) 331–337.
[20] J.H. Chae, K.H. Kim, Y.H. Choa, J.I. Matsushita, J.W. Yoon, K.B. Shim, Microstructural evolution of Al_2O_3–SiC nanocomposites during spark plasma sintering, J. Alloys Compds. 413 (2006) 259–264.
[21] L.R. Rossi, W.G. Lawrence, Elastic properties of oxide solid solutions: the system Al_2O_3–Cr_2O_3, J. Am. Ceram. Soc. 53 (11) (1970) 604–608.
[22] A. Harabi, T.J. Davies, Densification and grain growth in sintered alumina–chromia powder mixtures, Br. Ceram. Trans. 94 (1995) 97–102.